Combined Thermo-Reflectance and Thin-Film Coating in Near-Field Imaging of Chip-Package-PCB-Antenna Modules for Industrial-Testing and Failure Analysis

S. Wane[$], D. Kendig[†], T.V. Dinh[$], K. Alkhalifeh[$,*], A. E. Cabrera[$,⊥], Q.H. Tran[$], M. Shakouri[†], A. Shakouri[†], L. Salmon[⊥], G. Molnar[⊥], K. Ridier[⊥], D. Bajon[$], L. Nyssens[*], A. Pip[*], M. Vanbrabant[*], M. Rack[*], D. Tihon[*], C. Craeye*, P. Simon[*], J.-P. Raskin[*], D. Lederer[*], A. Bousseksou[⊥]

[$]eV-Technologies, France, [†]Microsanj LLC, USA, [⊥]LCC-CNRS, France, [*]UCL-ICTEAM, Belgium

***Abstract*—A holistic Near-Field (NF) Over-the-Air (OTA) testing solution for Chip-Package-PCB-Antenna modules based on combined thermo-reflectance and thin-film coating using Spin-Crossover (SCO) materials is proposed. The SCO coating process exhibits highly reliable thermometric performance (diffraction-limited sub-µm spatial, sub-µs temporal and 1°C thermal resolution), which stems to a large extent from the unprecedented quality of the vacuum-deposited thin films of the molecular complex used in this work. The resulting performance qualifies the SCO coating process, in terms of fabrication and switching endurance (surpassing 10^7 thermal cycles in ambient air), for industrial testing ensuring highly reproducible measurement results. The proposed NF sensing solutions are validated through several practical applications using front-end-modules (FEMs) manufactured in advanced GaN and FDSOI technologies co-designed with antenna-in-package (AiP) modules based on heterogeneous system-in-package (SiP) and WLCSP fan-in/fan-out integration assemblies.**

***Keywords*—Thermo-reflectance imaging, spin-crossover material, front-end-modules, beamforming, OTA testing, failure analysis, stochastic field-field correlation functions, physics-based deep-learning signal-processing.**

I. Introduction

Over the past decades, time-domain (TD) and frequency-domain (FD) thermo-reflectance imaging technologies have been established as mature and very powerful thermometry tooling solutions for characterizing the thermal properties of materials and circuit components with remarkable capabilities in pushing spatial resolutions to ultimate diffraction limits [1-3]. Beyond the interrogation of thermal properties of materials and circuit components, we introduce a *holistic Chip-Package-PCB-Antenna approach* for enabling ultra-fast (*500ps timescale*) thermal-imaging based industrial-testing and failure analysis at the module level. This technique fosters new near-field OTA testing solutions bridging electromagnetic fields representation with thermal imaging maps. To the best of our knowledge, this work represents the first holistic near-field *Chip-Package-PCB-Antenna* solution for industrial-testing and failure analysis at module level based on optical and thermal images with absolute temperature calibration. A large range of applications would benefit from the proposed unified near-field sensing technology, such as radiative cooling, thermophotovoltaic devices or the design of cheap but well controlled sources for photonic circuits, optical wireless communication (OWC), inter and intra-chip communications using photonics, satellite optical communication and LED beamsteering/beamforming.

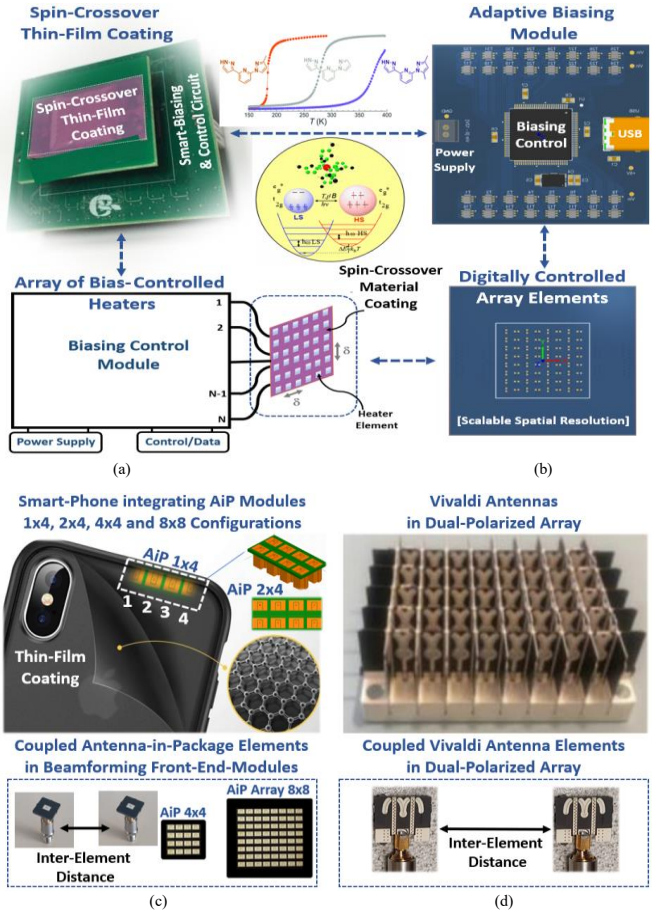


Fig. 1: Spin-Crossover thin-film coating (a) with controllable biasing (b) in combination with thermo-reflectance measurement solution for OTA testing of Chip-Package-PCB-Antenna modules. Antenna-in-Package (AiP) (c) and broadband Vivaldi antennas for beamforming applications (d).

In all aforementioned applications, dealing with electromagnetic sources in terms of their thermal footprints is a significant challenge due to the *partial spatial coherence* of the resulting fields [4],[5]. Thermally driven random fluctuations require the proper framework on the basis of stochastic field-field *correlation formalism*. Since numerical values cannot be specified for noise amplitudes, for modeling and measuring stochastic signals, it is required to deal with energy and power spectra through the extraction of auto and cross-correlation functions [6].

2023 IEEE Texas Symposium on Wireless and Microwave Circuits and Systems (WMCS) | 979-8-3503-3880-5/23/$31.00 ©2023 IEEE | DOI: 10.1109/WMCS58822.2023.10194284

979-8-3503-3880-5/23/$31.00 ©2023 IEEE

Authorized licensed use limited to: Univ Catholique de Louvain/UCL. Downloaded on November 30,2023 at 15:59:01 UTC from IEEE Xplore. Restrictions apply.

This contribution is built around two main sections. The first section describes the experimental setup of the proposed near-field OTA test solution including the calibration process for accurate extractions of absolute temperature accounting for device-sensor interactions. The second section is dedicated to practical applications based on the following use-cases:

- Beamforming modules co-designed with AiP array for 1×4, 1×8 and 8×8 MIMO channels for 26-30GHz applications.
- Co-design of a wideband FEM configurable balanced power amplifier in GlobalFoundries (GF) 22nm FD-SOI co-designed with a compact broadband AiP Vivaldi antenna-array with 5mm pitch for 24 - 43 GHz applications.

II. Main Results, Analysis and Discussion

A. *Principle of Proposed Instrumentation and Associated Calibration Solution*

- *Multi-Wavelength Thermo-Reflectance Measurement System: Accessible Spatial Resolution versus Near-Field Working Distance*

Fig. 2 shows the synoptic view of the near-field thermoreflectance measurement system [1-3]. The DUT's reflected illumination varies as a function of temperature. The laser acts as the DUT's heat source which is pulsed between on and off states. A high-resolution CCD camera quantifies the thermally induced optical reflectivity variations between the on and off states. The measurement results are cast in the form of a 2D spatial temperature distribution (thermal heatmap) that is obtained for each pixel.

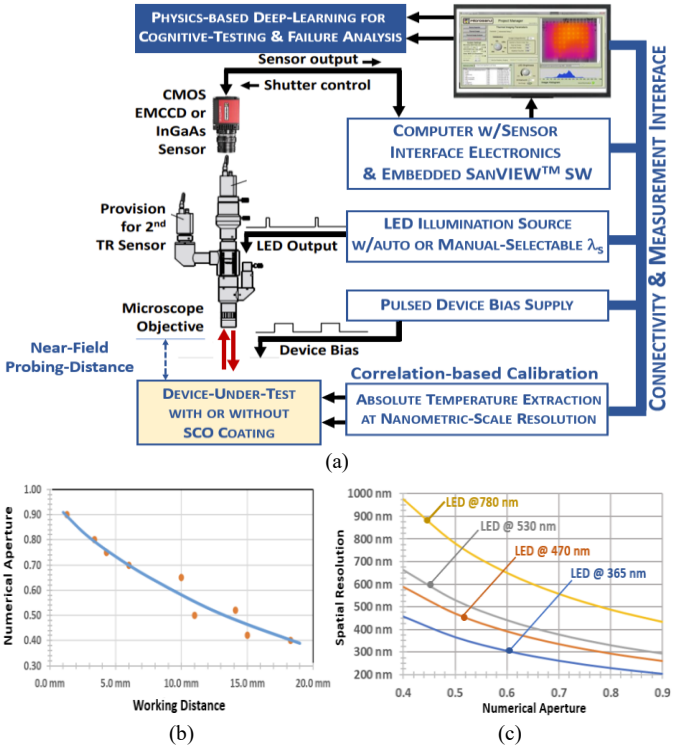


Fig. 2: (a) Synoptic view of proposed thermo-reflectance based OTA testing of Chip-Package-PCB-Antenna modules accounting for accurate absolute temperature calibration. (b) Numerical aperture NA as function of working distance and, (c) spatial resolution as function of NA [www.microsanj.com].

The use of an incoherent light source (LED) instead of a focused laser beam eliminates speckle or fringe type interference patterns that may occur with coherent illumination. Various modulation schemes can be used to detect the relative change in reflectivity of the surface of the DUT, including the homodyne method, the heterodyne method and transient effects. Fig. 2 (b) represents the numerical aperture (NA) as a function of the working distance (WD) while Fig. 2(c) shows the spatial resolution as a function of the numerical aperture. The WD is the distance between the front lens of the objective to the DUT surface when the inspected area is in focus thus defining the maximum measurement distance (DUT height). The resolution is defined by the shortest distance between two points that can still be separated. The NA defines the Point Spread Function (PSF), which is the light intensity distribution in the image acquired by the microscope from a point source. As the thermoreflectance coefficient is strongly dependent on the illumination wavelength, the choice of the LED is of significant importance in determining the sensitivity of CCD-based thermoreflectance. The relation between the relative change in reflectivity and the temperature variation can be approximated to a first order by the linear relation:

$$\frac{\Delta R}{R} = \left(\frac{1}{R}\frac{\partial R}{\partial T}\right)\Delta T = C_{th}\Delta T \qquad (1)$$

where C_{th}, typically on the order of 10^{-2} to 10^{-5} per °K, is the thermoreflectance coefficient. C_{th} depends on the DUT, the wavelength of the illuminating LED light, the angle of incidence (and thus, by extension, the surface roughness) and, in the case of multi-layer structures, the composition of the overall structure. In addition to providing accurate differential temperature ΔT, absolute temperatures can be extracted using thin-film SCO materials with nanometric spatial resolution.

- *Spin-Crossover Material with Functionalized Coating of Chip, Package, PCB and Antenna for Accurate Calibration of Absolute Temperature with Sub-µm Resolution*

The synthesized coating materials used in combination with thermo-reflectance sensing are based on quantum spin-crossover (SCO) materials exhibiting functional properties which are responsive to multi-physics external stimuli such as temperature, pressure, light irradiation, electromagnetic field, nuclear decay, soft-X-ray, and (de)solvation [7]. The following calibration structures have been designed, manufactured and characterized in a broad temperature range (from -40°C to +200°C):

1) Gold nanowires fabricated on glass and silicon wafers with controlled current sources.
2) Digitally controlled heating array-elements with scalable spatial resolution and power-levels.

The gold nanowires were fabricated on top of glass and oxidized silicon substrates, Si/SiO_2. The SiO_2 layer of the silicon substrate is 600-nm-thick. The fabrication of the nanowires and the electrodes was processed in two steps. First, E-beam lithography was used to pattern nanowire, then followed by the deposition of 10 nm Ti/50 nm Au bilayer. The chips were then completed with the second step using UV photolithography to pattern the electrodes and microwires connectors.

Authorized licensed use limited to: Univ Catholique de Louvain/UCL. Downloaded on November 30,2023 at 15:59:01 UTC from IEEE Xplore. Restrictions apply.

The material for the electrode and microwires is the deposited 10 nm Ti/300 nm Au bilayer. Ti layer is used as an adhesive layer due to its high transparency. Then the thermal-cycling and time-resolved experiments were performed for the SCO layers of 200 nm-thick coating on top of the chip. Details of the fabrication process were presented in [7].

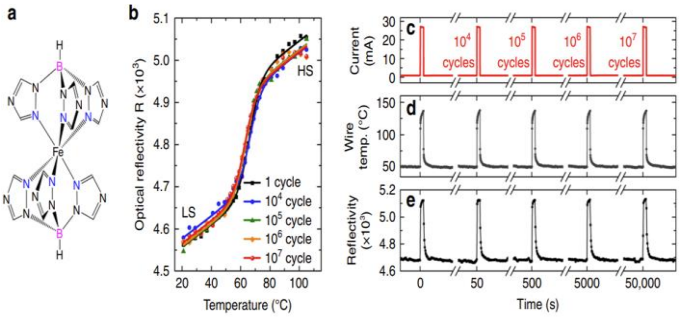


Fig. 3: Phase-change properties and switching endurance of the thin films. (a) Molecular structure. (b) Thermal evolution of the optical reflectivity (λ=452nm) of a 200-nm-thick film of 1 on top of a gold microwire (2mm×2µm×300nm) after 1, 10^4, 10^5, 10^6, and 10^7 thermal cycle in air induced by Joule heating. These data show the large variation of the reflectivity due to the molecular spin-state switching and demonstrate the exceptionally high resilience of the spin transition over 10^7 thermal cycles. Time evolution of (c) the applied electrical current, (d) the wire temperature, and (e) the optical reflectivity on the wire recorded simultaneously at selected times of the thermal-cycling experiment using the Joule-heated microwire. Results are from [7].

The chip was mounted on an adjustable-temperature microscope stage (Linkam Scientific Instruments, LTS120) to control and stabilize the temperature (Tb) of the entire circuit. To heat up the nanowire, the SCO-coated chip was connected to a low noise current source (Keithley 2611A), through an eight-track connector. In the experiments, the low noise current source is used to ensure the reproducibility of the Joule heating effect in the nanowires. Optical reflectivity images were recorded by a CCD camera (Andor Technology Clara, 1392×1040 pixels of 6.45µm size) equipped in an Olympus BX51 upright microscope. The ×50 or ×100 microscope objective lens (NA=0.5 and 0.9, respectively) were used. Time-resolved pump-probe reflectivity images were acquired using a gated intensified-CCD camera (Andor Technology iStar DH734) triggered by a function generator (Tektronix AFG3022C) allowing the generation of time-varying current pulses.

Dedicated hardware and software developments were conducted for accurate absolute temperature calibration (Fig. 4) using sensor-arrays with adaptive biasing for the regulation of the power dissipated through the individually controlled array-elements. A 64-element sensor-array (N=64, Nx=Ny= 8) was built using SMD-based heaters regulated using "Adaptive-Biasing". The sensor-array module includes:

- An $N = Nx \times Ny$ array of heating sensors with a spatial pitch of δ in the x and y directions.
- A biasing and control module for regulating the current flowing into the heating elements.
- A coated spin-crossover thin film with different thickness values.
- Control software for biasing the different heating elements.

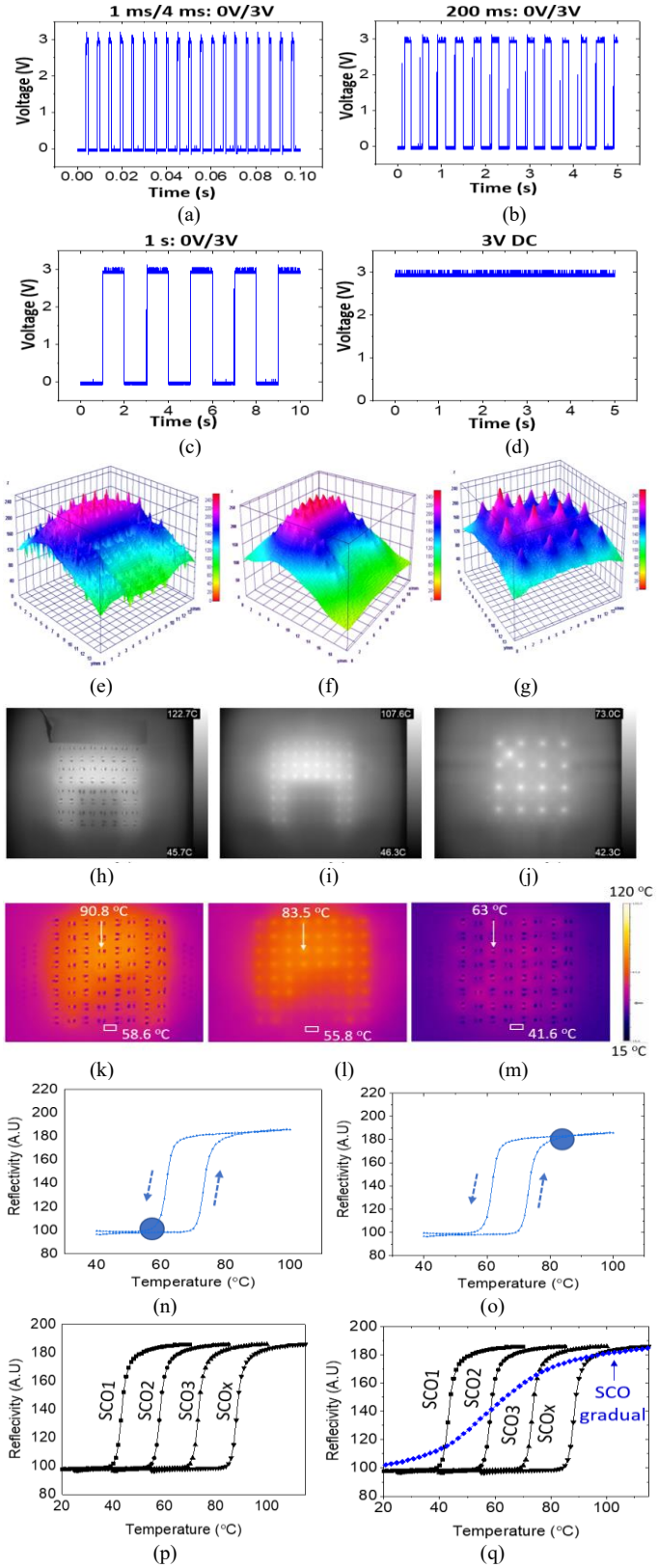


Fig. 4: Switched-biasing for absolute temperature calibration using SCO thin-film coating: time-domain voltage waveforms (a)-(d). Microsanj thermo-reflectance measurement of sensor-array heaters (e)-(j). IR-based imaging (k)-(m) for cross-verifications. Reflectivity *vs*. temperature hysteresis profiles of a SCO thin-film with controllable slopes for broadband calibration of absolute temperatures accounting for pixel-to-pixel interactions (n)-(q).

Authorized licensed use limited to: Univ Catholique de Louvain/UCL. Downloaded on November 30,2023 at 15:59:01 UTC from IEEE Xplore. Restrictions apply.

B. *Combined Thermo-Reflectance and Thin-Film Coating for High-Resolution Near-Field Imaging of Chip-Package-PCB-Antenna Modules*

Beamformer integrated circuits (IC) are essential building blocks of 5G/6G communication systems. These multiport devices integrate multi-directional transmit (Tx)/receive (Rx) channels into front-ends, which are integrated with antenna elements. The critical elements of beamformer ICs must be tested efficiently and thoroughly under multi-physics conditions (*linear and nonlinear conditions, across an entire workflow from design and verification/validation to manufacturing*). The design, dimensioning and testing of beamformer modules for single-beam and multi-beam high-throughput communications is a very challenging task in which the antenna, RF front-ends and host-PCB subsystems must be considered as a whole for achieving best performance with reliable mission profile. In the following sections, an efficient Thermo-Reflectance based imaging solution is proposed for *non-contact (OTA-compliant)* and *non-destructive* testing and failure analysis of *Chip-Package-PCB-Antenna* circuits and systems.

- *Near-Field Thermo-Reflectance Sensing of AiP Front-End-Modules for Beamforming Applications*

For RF/mmW testing of 5G user equipment (UE), the 3GPP has approved the use of a compact range, or compact antenna test range (CATR) operating as an indirect far-field (IFF) measurement system. The compact range uses a reflector to collimate the beam of a feed antenna to synthesize far-field conditions within a cylindrical area called the quiet zone (QZ). Figure 6(a) shows a CATR for a 50 cm QZ.

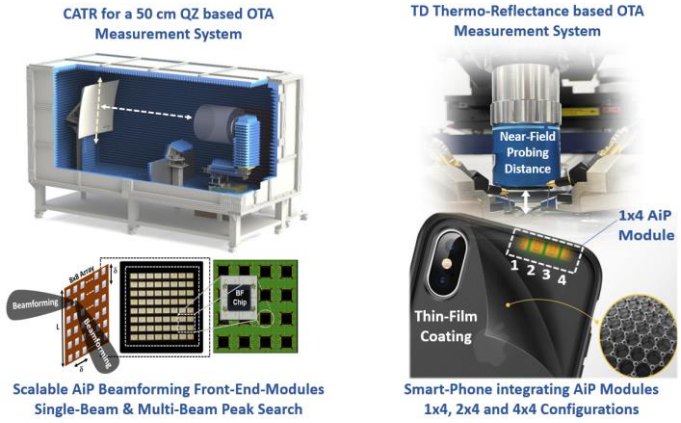


Fig. 5: CATR measurement setup (a), proposed thermo-reflectance based OTA testing solution (b) of Chip-Package-PCB-Antenna modules.

The QZ is shown as the gray cylinder domain. The compact range provides far-field conditions with dimensions much smaller than those of a conventional anechoic chamber. As long as the AUT is kept within the domain of the QZ, it will operate in far-field conditions without particular restrictions regarding surface currents or the size of an active subarray/module. However, the measurement time remains a significant challenge in addition to difficulties related to the possibility to identify faulty elements in an array of the beamformer module. In addition, classical antenna testing systems require a mechanical positioner for full angle-scanning.

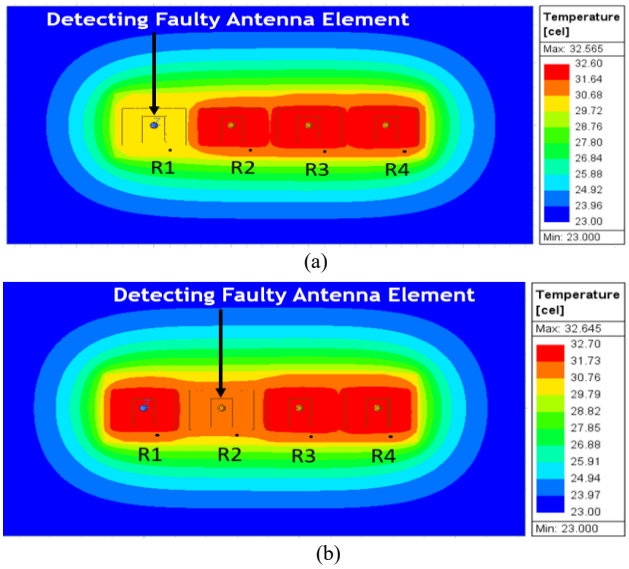


Fig. 6: Use of *Thermo-Reflectance* based EM-Thermal analysis for detecting faulty antenna elements in UE AiP devices: in (a) the faulty antenna is labelled as R1, in (b) the faulty antenna is labelled as R2.

Fig. 6 illustrates a simple and fast alternative testing solution that allows the diagnosis of faulty elements in antenna arrays using the proposed *Thermo-Reflectance* based EM-Thermal sensing technologies.

- *Thermo-Reflectance of Broadband Vivaldi AiP Module Co-Designed with Dual-Band Balanced PA Front-End-Module in GF 22nm FDSOI Technology*

Two power amplifiers (PAs) were designed in a 22nm FD-SOI CMOS technology. The first (PA1) is a wideband PA instantaneously covering the 5G 24-43GHz bands. The second (PA2) is designed in a balanced topology integrating PA1 with configurable hybrid couplers, covering the same frequency bands. They feature a high peak PAE of up to 36.4% and 28.3%, respectively, and saturated output powers of 18.6 and 20.1 dBm. Biased in deep class AB, their 1dB compression point performances are also close to saturation with 18.1 and 19.6dBm in P_{out} and 36.1 and 28.3% in PAE. In addition to compensating V_{th}-related process variations, the back-gate bias can shift the operating class and tradeoff AM-AM for AM-PM distortion. The PAs maintain good performance with a VSWR of 3:1, with peak PAE and P_{out} drops up to 15 and 11% and 2.3dB respectively in the 24-43 GHz bands. PA2 uses a balanced topology by combining two cells of PA1 with configurable 90° hybrid couplers (HCs) (see Fig. 7). Such balanced topology features increased output power and robustness to load variation but suffers from PAE degradation due to losses in the output HC. Small- and large-signal continuous-wave measurements were performed. A peak 27.7dB gain was achieved at 28GHz and a smaller local peak of 18.8dB at 44GHz (Fig. 8(a)-(c)). The 3dB-bandwidths associated with the low-and high-frequency peaks span from 24.7 to 30.5GHz and from 32.8 to 47.3GHz, respectively. The Dual-PA front-end is co-designed with a broadband Vivaldi antenna available in single-element and in array (4×4, 8×8) configurations for scalable MIMO applications.

Authorized licensed use limited to: Univ Catholique de Louvain/UCL. Downloaded on November 30,2023 at 15:59:01 UTC from IEEE Xplore. Restrictions apply.

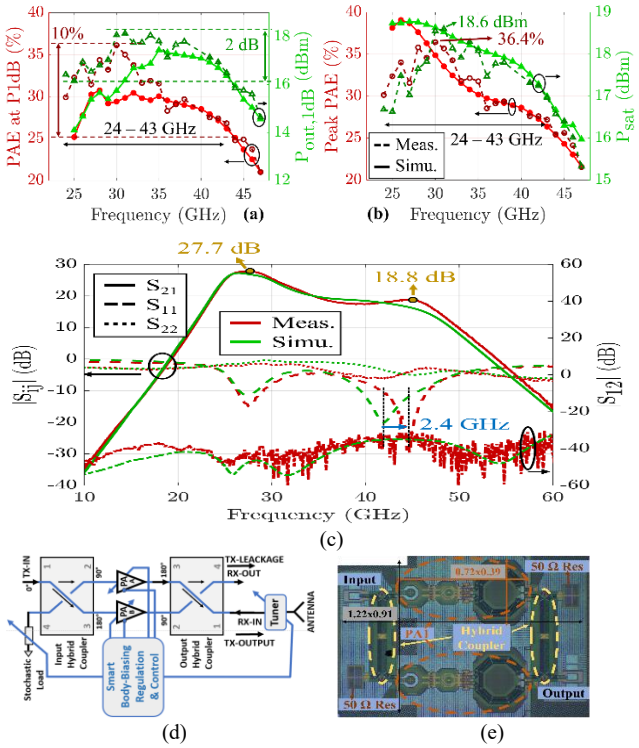


Fig. 7: Measurements in dark, dashed lines and simulations in light, solid lines. Nominal bias. PAE (left axis) and P_{out} (right axis) of the *PA1*, at 1dB CP (a) and at peak PAE (b). Measured and simulated S-parameters (c) of *the Dual-PA* (d)-(e) manufactured using GF 22nm FDSOI technology.

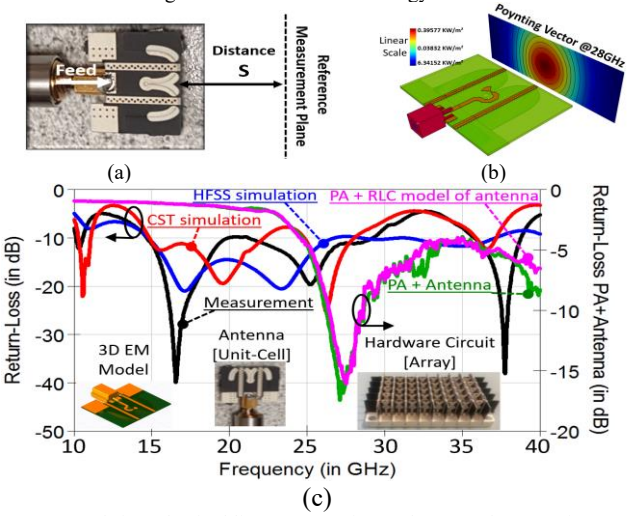


Fig. 8: (a) Fabricated Vivaldi antenna unitary element. (b) Poynting vector visualization at 28GHz. (c) Broadband measurement of return-loss of Vivaldi antenna elements in beamforming array compared to simulations using ASYS and CST.

It is observed that a direct link can be established between the thermal variations on the SCO coating material and the square of the electric (or magnetic) field. Few tens of dBm input power feeding the radiating elements will generate a few degrees heating dynamics from which field amplitudes can be deduced from the power density (*spatially averaged*) in the form:

$$|sPD| = \propto X_{EM-Thermal}^{Power-Density} \Delta T_{Averaged} \qquad (2)$$

In (2) $X_{EM-Thermal}^{Power-Density}$ links differential temperature $\Delta T_{Averaged}$ to EM-fields based power-density (*Poynting vector*).

Fig. 9(a)-(b) present near-field measurements of temperature distribution in transient mode using *Microsanj* Thermo-Reflectance platform at 28GHz for 30dBm input power. 3D full-wave EM-Thermal models of the antenna module are built using *ANSYS* (Fig. 9(c)-(d)) and compared to *Microsanj* measurement showing satisfactory results. Observed differences are attributed to adaptor transitions and frequency-dependent effects of thermal properties used in the stackup of the antenna module.

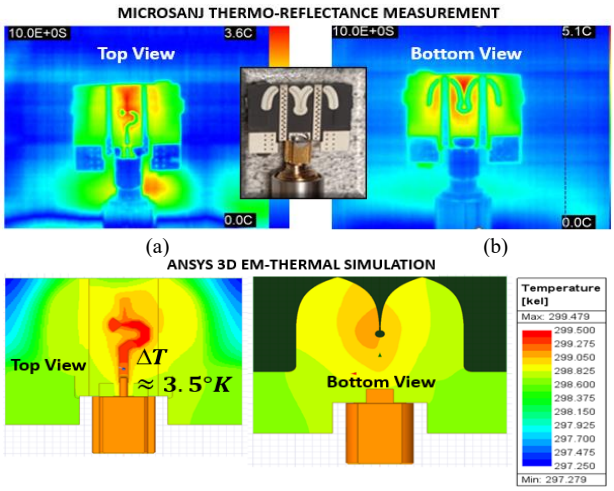


Fig. 9: Thermal heatmaps on Vivaldi AiP module for Beamforming applications in the band 15-40GHz: Measurement (a)-(b) using Microsanj versus 3D EM-Thermal simulations using ANSYS (c)-(d).

We introduce a correlation-aware RLC synthesis solution for linking electromagnetic theory-based fundamental analysis of wireless communication systems to classical circuit-theory based on Kirchhoff laws, properly accounting for impedance matching, interference and coupling between noisy radiating elements.

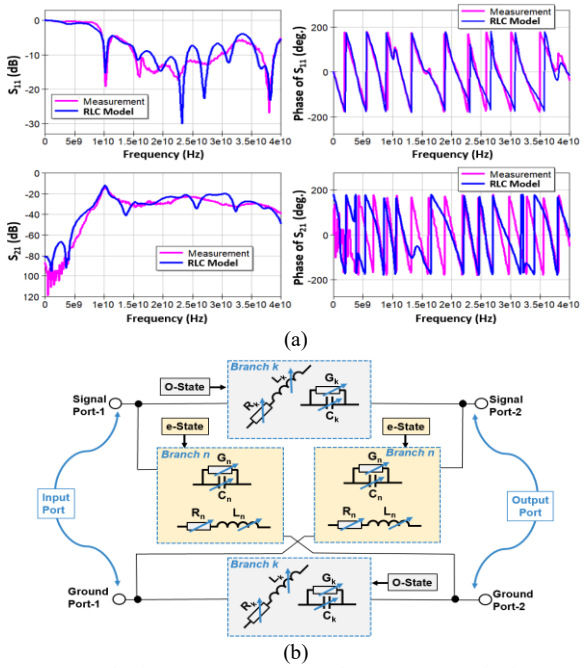
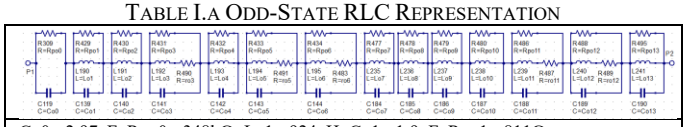


Fig. 10: RLC-synthesis versus measurement for (a) S11-magnitude, S11-phase, S21-magnitude, and S21-phase. Broadband power-dependent RLC-synthesis (b) of coupled Vivaldi antennas.

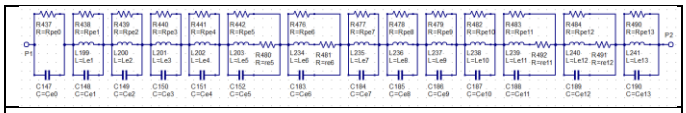
Authorized licensed use limited to: Univ Catholique de Louvain/UCL. Downloaded on November 30,2023 at 15:59:01 UTC from IEEE Xplore. Restrictions apply.

TABLE I.A ODD-STATE RLC REPRESENTATION



Co0 =2.97pF, Rpo0 =348kΩ, Lo1 =924pH, Co1 =1.9pF, Rpo1 =811Ω
Lo2 =219pH, Co2 =2pF, Rpo2 =591Ω, Lo3 =47.8pH, Co3 =5pF
Rpo3 =44.8Ω, ro3 =0.1Ω, Lo4 =130pH, Co4 =1.5pF, Rpo4 =167Ω
Lo5 =43.9pH, Co5 =2.5pF, Rpo5 =91.4Ω, ro5 =0.1Ω, Lo6 =94.3pH
Co6 =1pF, Rpo6 =93.4Ω, ro6 =0.1Ω, Lo7 =63.3pH, Co7 =0.9pF
Rpo7 =77.9Ω, Lo8 =26.8pH, Co8 =1.6pF, Rpo8 =97.7Ω, Lo9 =29.8pH
Co9 =1.1pF, Rpo9 =78.4Ω, Lo10 =24.3pH, Co10 =1pF, Rpo10 =151Ω
Lo11 =9.11pH, Co11 =2pF, Rpo11 =73.6Ω, ro11 =0.02Ω, Lo12 =16.1pH
Co12 =1pF, Rpo12 =138Ω, ro12 =0.03Ω, Lo13 =28.7pH, Co13 =0.5pF, Rpo13 =100Ω

TABLE I.B EVEN-STATE RLC REPRESENTATION



Ce0 =2.97pF, Rpe0 =217kΩ, Le1 =924pH, Ce1 =1.9pF, Rpe1 =810Ω
Le2 =219pH, Ce2 =2pF, Rpe2 =797Ω, Le3 =50.7pH, Ce3 =5pF
Rpe3 =84.3Ω, Le4 =128pH, Ce4 =1.5pF, Rpe4 =217Ω, Le5 =44.5pH
Ce5 =2.5pF, Rpe5 =96.4Ω, re5 =0.1Ω, Le6 =94.3pH, Ce6 =1pF
Rpe6 =86.8Ω, re6 =0.2Ω, Le7 =53.8pH, Ce7 =1.1pF, Rpe7 =80.5Ω
Le8 =39.7pH, Ce8 =1.1pF, Rpe8 =73.4Ω, Le9 =29pH, Ce9 =1.1pF
Rpe9 =91.3Ω, Lo10 =24.3pH, Co10 =1pF, Rpo10 =151Ω, Le11 =9.16pH
Ce11 =2pF, Rpe11 =77Ω, re11 =0.02Ω, Le12 =16.1pH, Ce12 =1pF
Rpe12 =146Ω, re12 =0.03Ω, Le13 =28.7pH, Ce13 =0.5pF, Rpe13 =100Ω

The proposed correlation-aware RLC synthesis solution is built using eigen-states EM-based modal representation accounting for distributed floating local ground references. The ability of the proposed solution to map physical design parameters into a broadband physics-based RLC equivalent circuit model is demonstrated using parameterizable SPICE-netlist with the following attributes:

- Meaningful interpretation of synthesized RLC elements.
- Broadband accuracy with minimal complexity.
- Preservation of passivity and causality.

The comparison (in Fig.10(a)) between synthesized broadband RLC model using eigen-states based X-topology architecture (Fig.10(b)) and measurement shows excellent agreement.

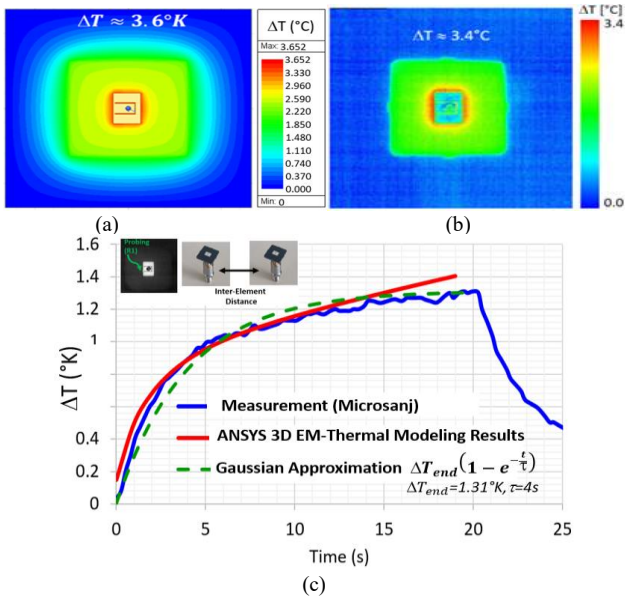


Fig. 11: Thermal distribution on AiP module for beamforming applications in the band 26-30GHz: 3D EM-Thermal simulations (a) using *ANSYS* versus measurement (b) using Microsanj in transient mode (c).

Use of broadband physics-based RLC model representation accounting for thermal dependency opens new possibilities in using thermo-reflectance imaging solutions for anticipating potential failures at module-level before they happen, and for predicting their remaining lifespan before failure. Broadband RLC representations also create bridges with time-domain linear/nonlinear analyses. Fig. 11 shows good alignment between thermo-reflectance based time-domain measurements and *ANSYS* full-wave 3D EM-thermal simulations.

III. CONCLUSION

We have proposed a new holistic Near-Field (NF) Over-the-Air (OTA) testing solution for *Chip-Package-PCB-Antenna* modules based on combined *Thermo-Reflectance* and *Thin-Film coating* using *Spin-Crossover (SCO)* materials. The SCO coating process demonstrates highly reliable thermometric performance qualifying it, in terms of fabrication and switching endurance (*surpassing 10^7 thermal cycles in ambient air*), for industrial testing ensuring highly reproducible measurement results. The proposed solution is demonstrated with front-end-modules manufactured in advanced GaN and FDSOI technologies co-designed with AiP on WLCSP fan-in/fan-out integration assemblies.

Among the advantages of the proposed Thermo-Reflectance based testing are the following differentiating attributes:

- No need for mechanical positioner/step-motor system.
- Ultra-fast test-time compliant with mass-market industrial requirements.
- Unified functional and reliability testing solution based on a holistic Chip-Package-PCB-Antenna approach.
- High accuracy absolute temperature calibration using SCO thin-film coating with sub-µm spatial resolution.
- No disturbing RF/mmW interference between the DUT and the probing system to be deembedded.
- Suitable for physics-based RLC extractions in conjunction with deep-learning algorithms for full test-coverage including ESD and electromigration compliance requirements.

REFERENCES

[1] A. Shakouri, "SiGeC/Si superlattice microcoolers," Appl. Phys. Lett., vol. 78, pp. 1580-1582, 2001.

[2] K. Yazawa, D. Kendig, P. Raad, P. Komarov and A. Shakouri, "Understanding the thermoreflectance coefficient for high resolution thermal imaging of microelectronic devices," Technical Brief, Electronics Cooling Magazine, vol. 2013, pp. 10-14, 2013.

[3] D. Kendig, et al., "Hyperspectral thermoreflectance imaging for power devices," in Annual IEEE Semiconductor Thermal Measurement, Modeling, & Manag. Symp. (Semi-Therm) (IEEE, 2017), pp. 204–207.

[4] Denis Tihon, et al., "Modal characterization of thermal emitters using the Method of Moments", EuCAP, 2020, pp. 1-5.

[5] E. Wolf, "New theory of partial coherence in the space–frequency domain. Part I: Spectra and cross spectra of steady-state sources". J. Opt. Soc. Am. 1982, 72, 343–351.

[6] S. Wane, et al., "Correlation Technologies for Emerging Wireless Applications". Electronics 2022, 11, 1134. https://www.mdpi.com/2079-9292/11/7/1134.

[7] K. Ridier, et al., "Unprecedented switching endurance affords for high-resolution surface temperature mapping using a spin-crossover film", Nature Communications, vol. 11, 2020. https://doi.org/10.1038/s41467-020-17362-7.

Authorized licensed use limited to: Univ Catholique de Louvain/UCL. Downloaded on November 30,2023 at 15:59:01 UTC from IEEE Xplore. Restrictions apply.